OPEN

Quasi-hydrostatic equation of state of silicon up to 1 megabar at ambient temperature

Simone Anzellini[1]*, Michael T. Wharmby[1,2], Francesca Miozzi[3], Annette Kleppe[1], Dominik Daisenberger[1] & Heribert Wilhelm[1,4]

The isothermal equation of state of silicon has been determined by synchrotron x-ray diffraction experiments up to 105.2 GPa at room temperature using diamond anvil cells. A He-pressure medium was used to minimize the effect of uniaxial stress on the sample volume and ruby, gold and tungsten pressure gauges were used. Seven different phases of silicon have been observed along the experimental conditions covered in the present study.

Silicon is one of the most studied elements in the world for its use in microelectronics, semiconductors technologies and its importance in Earth science[1,2]. For example, it is believed that a certain percentage of Si could be contained in the Earth's core together with Fe and Ni and other light elements (such as S, O, H and C)[3]. For these reasons, Si has been extensively studied (experimentally and theoretically) under extreme conditions and so far up to seven different polymorphs have been observed in compression experiments at ambient temperature.

At ambient conditions Si presents a diamond structure ($Fd\overline{3}m$) labeled as Si-I. Under increasing pressure, Si-I transforms, via a coexistence region, into the metallic Si-II phase with a tetragonal β-Sn structure ($I4_1/amd$)[4]. The observed transition pressure from Si-I to Si-II and the pressure range over which coexistence is observed, strongly depend on the experimental conditions and they are both affected by non-hydrostatic stresses. In Diamond Anvil Cell (DAC) experiments performed using different techniques (from X-ray diffraction (XRD) to Raman), the reported Si-I/II transition pressure varies from 8.8 to 12.5 GPa[5–10]. Under uniaxial compression, the reported phase transition has been shown to occur at 12 GPa along the [100] and at lower pressure along the [111] direction via electrical resistance measurement[11]. Under shock compression, instead, the transformation is observed in the 6–14 GPa pressure range[12–15].

In a DAC experiment using a 4:1 methanol:ethanol mixture as pressure medium, McMahon et al. observed a new phase transition from the β-Sn structure to an orthorhombic phase (space group $Imma$) at a pressure of 14.4 GPa[6]. The new phase, named Si-XI, remains stable up to 16 GPa, when the structure transforms to a simple hexagonal ($P6/mmm$) phase named Si-V[6,10]. Under further compression, Si-V converts to the orthorhombic Si-VI phase ($Cmca$) at a pressure of 37.6 GPa. This phase was first observed by Olijnyk et al.[10] and subsequently indexed as a large orthorhombic cell, containing 16 atoms, by Hanfland et al.[16]. In the pressure range 40–42 GPa, the structure undergoes a further phase transition to the Si-VII ($P6_3/mmc$) form, which remains stable up to 79 GPa[17]. Above this pressure, the cubic phase Si-X ($Fm\overline{3}m$) develops which is stable up to at least 243 GPa[17].

Although the characterization of the high temperature part of the phase diagram of Si is beyond the scope of the present paper, a comprehensive description of the experimental and theoretical works performed so far on Si can be found in the articles of Turneaure et al.[18] and Paul et al.[19]. Under decompression at ambient temperature, four additional phases have been observed to form from Si-II. In particular, under rapid decompression of Si-II to atmospheric pressure, the tetragonal phases Si-VIII ($P4_12_12$) and Si-IX ($P4_22_2$) appear[20]. Upon relative slow decompression, Si-II transforms instead around 8–10 GPa into a semiconducting phase with a rhombohedral R8 structure (Si-XII)[21] which in turn transforms after further decompression into the Si-III phase, with a body-centred cubic BC8 unit cell[22].

Although Si has been extensively studied using several experimental and theoretical techniques, most of the studies performed so far were focused more on the determination of the pressure domain of a particular phase

[1]Diamond Light Source Ltd, Diamond House, Harwell Science and Innovation Campus, Didcot, OX11 0DE, UK. [2]PETRA III, Deutsches Elektronen-Synchrotron (DESY), Notkestrabe 85, 22607, Hamburg, Germany. [3]Sorbonne Université, UMR CNRS 7590, Muséum National d'Histoire Naturelle, Institut de Minéralogie, de Physique des Matériaux et de Cosmochimie, IMPMC, 75005, Paris, France. [4]Helmoltz Institut Ulm, Helmhotzstrβe11, D-89081, Ulm, Germany. *email: simone.anzellini@diamond.ac.uk

(or several phases)[5,16,23–25]. A synchrotron XRD characterization of the complete compression curve of Si at ambient temperature by modern DAC techniques has never been performed. To our knowledge, the most recent experimental determination of the Si equation of state (EOS) is from 1990[17]. In these experiments the Si EOS was investigated by energy dispersive XRD from 40 to 243 GPa without any pressure medium. Since then, great progress has been achieved in the accuracy of the determination of compression curves. In particular the use of helium as a pressure transmitting medium has meant that samples experience a higher hydrostatic stress during the experiment[26]. Third generation synchrotron sources have permitted smaller beam sizes with higher X-ray fluxes to be used, allowing for smaller sample sizes with more homogenous pressure in the illuminated region. Finally, the systematic uncertainties of DAC pressure metrology have been reduced, most importantly for the ruby pressure gauge[27]. In the last few years it has been shown that results obtained by modern synchrotron DAC techniques can significantly improve on those obtained by older methods[27–29]. These considerations have lead us to re-examine the Si compression curve at ambient temperature. To the best of our knowledge, this compression curve has never been investigated across the complete range from ambient to pressures greater than 1 MBar using the same method. By using helium (He) as a pressure transmitting medium we may observe changes in the sequence of phases formed, in line with those predicted by theory. Thus we will be able to better constrain the pressure domains of each phase under hydrostatic conditions.

Results

The structural evolution of crystalline Si from ambient pressure to 105.2 GPa has been investigated at ambient temperature under quasi-hydrostatic conditions. Over this pressure range, Si was observed to undergo six phase transitions four of which are associated with a coexistence region. In the following sections, the stability field and compression curve of each phase are described and compared with previous studies. The crystallographic changes occurring in the structures and the corresponding mechanisms of the phase transitions are well known, therefore they are not discussed in this paper. A comprehensive description of the phase transitions of the group IV elements has been previously presented by Katzke et al.[30].

Si-I: diamond structure.   At ambient pressure, the observed signal on the image plate presents a single crystal like texture corresponding to the 111, 311, 331, 422 and 511 reflections of the Si-I phase (diamond, $Fd\bar{3}m$). Under the present experimental conditions, the Si-I phase can be observed up to 13.9 GPa although a coexistence with the phases Si-II and Si-XI appears between 13.1 GPa and 13.5 GPa and will be discussed in detail later in the text.

During the data analysis, each (unsaturated) single crystal XRD peak was integrated individually and used to determine the lattice parameters for each reflection. The final value of the Si-I lattice parameter was then calculated as the average of all the measured ones.

In Table 1 the obtained results for Si-I are reported together with the corresponding pressure measured from the ruby fluorescence method[28]. Pressure measured from the compression curves of Au[31] and W[28] are also reported in the table to compare the reliability of the measured pressure and, to further constrain the pressure distribution inside the high pressure chamber during the experiment.

In Fig. 1 the corresponding normalized volumes per unit cell of the Si-I phase are plotted as a function of pressure together with the results obtained from previous studies. Si-I bulk modulus K_0, its pressure derivative K'_0 and the volume V_0 at ambient pressure have been determined by a least-squares fit of the present pressure-volume data to a Rydberg-Vinet[32] and a third-order Birch-Murnaghan (BM3) EOS[1].

The resulting values are summarized in Table 2. The uncertainties in the obtained values correspond to the 95 % confidence interval of the fitted values. When K'_0 is fixed to 4.24 as obtained in the ultrasonic measurement of McSkimin et al.[33], the obtained fit values are in good agreement with the ultrasonic ones (see Table 2).

In Table 2 the values obtained in this experiment are compared to the ones obtained from previous studies together with the observed pressure domain of pure Si-I phase. It is interesting to observe that the K_0 obtained in the present study by fixing K'_0 to the ultrasonic values of Mcskimin at al.[33], results 2.7% smaller than the ones calculated by Hennig et al.[34] in a DFT study using a Heyd-Scuseria-Ernzerhof screening Coulomb hybrid functional (HSE06). Whereas, the K_0 values obtained with DFT calculations using a generalized gradient approximation (GGA) and a local density approximation (LDA) in Wang et al.[35] are 9.5% and 2% lower than the one obtained in the present study (fixing K'_0), respectively.

The EOS derived from the compression curve of Si-I in the present work (Fig. 1) is in good agreement with the reported curve of McMahon et al.[6]. We note that in that work the authors report a phase transition to Si-II at 11.0 GPa, whereas in the present study no phase transition was observed before 13.1 GPa. A good agreement is also observed with the data of Senoo et al.[24] obtained with XRD experiment performed in a hydraulic press-driven cubic anvil apparatus using a 1:1 mixture of ethyl- and methyl-alcohols and, with the data obtained from an energy dispersive XRD experiment in 4:1 methanol:ethanol performed by Olijnyk et al.[10].

Hu et al.[5,36] also studied the compression of Si in a XRD-DAC experiment in 4:1 methanol:ethanol mixture. Comparing their result with the present study it is clear they are making an overestimation, despite their using the values derived from the ultrasonic studies of Mcskimin et al.[33]. Furthermore such an overestimation becomes more evident with increasing pressure with a percentage difference from the ultrasonic EOS passing from 0.27% at 3 GPa to 1.48% at 12.6 GPa. This trend is normally associated to a non-hydrostatic condition in the high pressure chamber of a DAC such as a direct compression of the sample between the diamond anvils[37].

Si-I, II and XI: first coexistence region.   The Si-I phase (cubic diamond structure, $Fd\bar{3}m$) is stable up to a pressure of 13.1 GPa when new peaks, associated to the tetragonal β-tin ($I4_1/amd$, Si-II) and the orthorhombic $Imma$ (Si-XI) phases, develop in addition to the five reflections of the cubic diamond phase (see Fig. 2). A similar behaviour has been previously observed by McMahon et al.[6], although they only discuss the possibility of a

Run	P_{ruby}[28]	Pau[31]	P_W[28]	a_{Au} (Å)	a_W (Å)	a (Å)
ST1	0.3		0.1		3.164	5.424
	0.5		0.4		3.163	5.423
	5.4		5.1		3.148	5.343
	10.1		9.5		3.134	5.279
ST3	2.1	2.1		4.062		5.392
	6.9	6.9		4.029		5.319
	11.0	10.9		4.004		5.264
	11.2	11.1		4.003		5.261
	11.3	11.2		4.002		5.260
	11.4	11.3		4.002		5.259
	11.5	11.4		4.001		5.257
	11.6	11.5		4.000		5.256
	11.7	11.6		3.999		5.255
	11.8	11.6		3.999		5.254
	11.9	11.6		3.999		5.254
	12.0	11.9		3.998		5.252
	12.6	12.4		3.995		5.245
	12.8	12.6		3.994		5.242
	13.0	12.9		3.993		5.240
	13.2	13.0		3.992		5.239
	13.3	13.1		3.991		5.239
	13.5	13.1		3.991		5.237
ST2	0.2	0.1		4.078		5.428
	0.4	0.4		4.075		5.423
	0.6	0.6		4.074		5.420
	1.7	1.6		4.066		5.404
	2.3	2.2		4.061		5.393
	3.0	2.9		4.056		5.380
	4.1	4.0		4.048		5.364
	5.5	5.5		4.038		5.340
	7.1	7.2		4.027		5.321
	8.9	8.9		4.016		5.298
	10.1	10.1		4.009		5.279
	10.6	10.5		4.006		5.273
	11.5	11.5		4.000		5.261
ST1-2	0.0					5.431
	2.2					5.393
	11.7					5.258
	12.3					5.251
	12.5					5.247
	12.6					5.246
	12.8					5.244
	12.9					5.243
	13.2					5.240

Table 1. Measured pressures in GPa and lattice parameters of tungsten (a_W), gold (a_{Au}) and Si-I for the four experimental runs. The data are listed in the order they have been taken. Experimental uncertainty on lattice parameters is lower than 0.003 Å. Uncertainty on pressure measurement increases from 0.05 GPa at 1 GPa to 2 GPa at 150 GPa if the ruby pressure scale is assumed to be correct[47].

coexistence of the three phases due to the overlapping of several peaks that can belong to both the *Imma* and the β-tin but couldn't be discriminated due to signal resolution problems. The coexistence of these three phases, has also been predicted by DFT simulations by Yao and Klug[38]. They found that up to a pressure of 10 GPa, the diamond structure is the most enthalpically favourable. From 10 GPa up to 13.2 GPa, the β-tin and the *Imma* structures are the most stable structures, both with similar enthalpies, whilst above this range the *Imma* structure becomes more favourable.

Table 3 reports the measured pressure domain of the Si-II and Si-XI phases together with the ones obtained from previous studies.
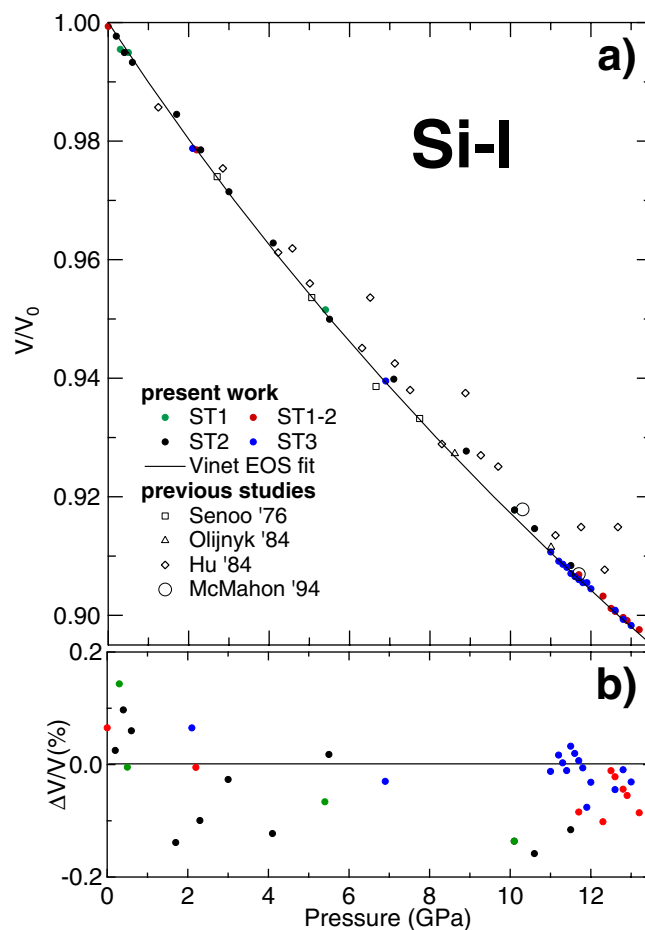
Figure 1. (**a**) Measured volume of Si-I as a function of pressure compared to previous experimental studies[6,10,24,36]. (**b**) Percentage error between the measured and fitted volume of the present data using a Vinet EOS with $V_0 = 20.031$ Å^3/atom, $K_0 = 97.89$ GPa and $K_0' = 4.24$.

Reference	V_0 (Å^3/atom)	K_0, K_0' (GPa)	P range (GPa)	PTM	Pressure gauge	EOS	Method
This Study	20.021	101.5, 3.43	0.0–13.0	He	Ruby[28], W[28], Au[31]	Vinet	XRD in DAC
This Study	20.037	96.50, 4.24*	0.0–13.0	He	Ruby[28], W[28], Au[31]	Vinet	XRD in DAC
This Study	20.011	101.5, 3.45	0.0–13.0	He	Ruby[28], W[28], Au[31]	BM3	XRD in DAC
This Study	20.037	96.86, 4.24*	0.0–13.0	He	Ruby[28], W[28], Au[31]	BM3	XRD in DAC
[6]	20.012	99.90, 3.80	0.0–11.7	4:1 methanol-ethanol	Ruby[7]	BM	XRD in DAC
[33]		97.88, 4.24	0.0–0.2				ultrasonic
[24]		96.00, 3.90	0.0–9.0	1:1 ethyl-methyl-alcohol	NaCl	M	hydraulic press
[5,36]		97.88, 4.24+	0.0–11.3	4:1 methanol-ethanol, Ar	Ruby[48] or NaCl		XRD in DAC
[49]		97.83, 5.08		He	Ruby[48]		PI in DAC
[10]			0.0–8.8	4:1 methanol-ethanol	Ruby[50]		ED-XRD in DAC
[35]	19.750	94.34, 4.08					DFT with LDA
[35]	20.510	87.29, 4.06					DFT with GGA
[34]	20.070	99.10, 4.00				BM	DFT with HSE06

Table 2. EOS parameters of Si-I measured (or calculated) in different experiments. The volume V_0, bulk modulus K_0 and its pressure derivative K_0' are listed. Experimental methods and EOS formulation are specified. The pressure range refers to regions where only the Si-I phase is observed. *: Fixed parameter. +: According to[5] their data are in agreement with the ultrasonic values from Mcskimin *et al.*, they didn't perform any actual fit. PTM: Pressure transmitting medium. M: Murnaghan. BM: Birch-Murnaghan. PI: Phonon Imaging.
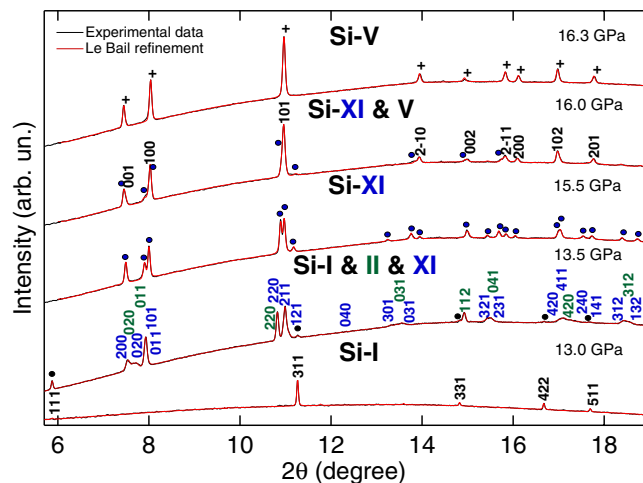
Figure 2. Le Bail refinements of XRD patterns collected in the ST3 run at 13.0 GPa, 13.5 GPa, 15.5 GPa, 16.0 GPa and 16.3 GPa representing the Si-I phase, coexistence between Si-I, II and XI, the Si-XI phase, coexistence between Si-XI and Si-V and the Si-V phase, respectively. All the phases have been indexed with different colours. The same colour code is used with the circle and crosses of the already indexed peaks. The 111 peak at 13.0 GPa was not included in the fitting as the single-crystal like reflection saturated the detector.

P domain	P′ domain	exp. type	PTM		Ref.
Si-II					
13.1–14.3	13.1–14.3	XRD in DAC	He		present
11.2–16.4	11.3–16.5	XRD in DAC	4:1 meth:eth		[36]
8.8–16.0	8.9–16.6	ED-XRD in DAC	4:1 meth:eth		[10]
11.7–14.4	12.0–14.8	XRD in DAC	4:1 meth:eth		[6]
11.0–13.6		DFT	N/A		[19]
Si-XI					
13.1–16.0	13.1–16.0	XRD in DAC	He		present
13.1–16.1	13.4–16.7	XRD in DAC	4:1 meth:eth		[6]
13.6–16.0		DFT	N/A		[19]

Table 3. Measured pressure domains for phases Si-II and XI compared to previous studies. In the table, P refers to the reported pressure domain while P′ is the pressure domain obtained by re-interpreting each reported data using the calibration used in the present study. PTM: Pressure transmitting medium.

Under the present experimental conditions, the onset of the phase transition from Si-I to Si-II (13.1 GPa) is higher than previously observed in other static compression experiments. The corresponding pressure domain of Si-II is narrower and, actually corresponds to the observed coexistence region between Si-II and XI reported by McMahon et al.[6,23]. The onset of the phase transition to Si-XI is also in good agreement with the results of McMahon et al.[6,23] while the observed pressure domain of Si-XI appears to be slightly narrower but in agreement within the experimental errors.

Although the β-tin and Imma phase reflections are strongly overlapping, it was possible to determine the lattice parameters for all three phases at the transition pressure via a Le Bail fit. The results obtained from the fit together with the measured pressure for both Si-II and Si-XI phases are reported in Table 4.

In Fig. 2, the reported integrated diffraction patterns and the corresponding Le Bail fits, show the structural evolution of Si from 13.0 GPa to 16.3 GPa. It is important to emphasise that at 13.5 GPa only by considering the three phases (I,II and XI) together can explain the observed reflections. Also interesting is the different behavior of the 020, 211 and 121 reflections of the Si-XI phase from 13.5 GPa to 15.5 GPa. At 13.5 GPa, when the three phases coexist, the 020 reflection of Si-XI is closer to the 200, while the 211 and 121 are overlapped, forming a single broad peak. At 15.5 GPa, however, when only the Si-XI phase is observed, the 020 reflection appears to be closer to the 101 and the 211 and 121 are well separated in two distinct peaks as previously reported[6]. Detailed XRD refinements of the coexistence region are reported from Fig. S8 to Fig. S17 of the Supplementary Materials.

In the compression curves obtained for both phases (Fig. 3) we observe a plateau corresponding to the coexistence region. In the region with only the Si-XI phase, a decreasing trend in the compression curve is observed.

| P$_{ruby}$[28]	P$_{Au}$[31]	a$_{Au}$ (Å)	phase	a(Å)	b(Å)	c(Å)
ST3						
13.5	13.1	3.990	II	4.648		2.560
13.6	13.2	3.990	II	4.648		2.560
13.8	13.3	3.989	II	4.647		2.559
13.9	13.5	3.988	II	4.645		2.557
14.0	13.6	3.987	II	4.644		2.558
14.1	13.7	3.987	II	4.642		2.557
13.5	13.1	3.990	XI	4.714	4.601	2.545
13.6	13.2	3.990	XI	4.714	4.603	2.543
13.8	13.3	3.989	XI	4.714	4.601	2.544
13.9	13.5	3.988	XI	4.713	4.594	2.550
14.0	13.6	3.987	XI	4.714	4.587	2.555
14.1	14.0	3.985	XI	4.716	4.586	2.554
14.3	13.9	3.986	XI	4.712	4.575	2.558
14.4	14.0	3.985	XI	4.717	4.568	2.557
14.5	14.4	3.983	XI	4.718	4.562	2.558
14.6	14.3	3.984	XI	4.723	4.554	2.558
14.7	14.6	3.982	XI	4.726	4.545	2.556
14.9	14.8	3.981	XI	4.730	4.538	2.556
15.0	14.6	3.982	XI	4.734	4.530	2.555
15.2	14.8	3.981	XI	4.737	4.520	2.555
15.3	14.9	3.980	XI	4.740	4.511	2.524
15.5	15.1	3.980	XI	4.743	4.503	2.553
15.7	15.2	3.979	XI	4.748	4.491	2.553
15.8	15.4	3.978	XI	4.748	4.479	2.551
16.0	15.5	3.977	XI	4.761	4.461	2.553
16.1	15.7	3.976	XI	4.778	4.427	2.550
ST2						
13.1	13.0		II	4.656		2.556
13.4	13.2		II	4.653		2.546
14.3	14.1		II	4.644		2.556
13.1	13.0		XI	4.708	4.606	2.555
13.4	13.2		XI	4.707	4.599	2.554
14.3	14.1		XI	4.700	4.591	2.561
15.3	15.2		XI	4.738	4.517	2.553
16.0	15.9		XI	4.764	4.472	2.549

Table 4. Measured pressures in GPa and lattice parameters of gold (a$_{Au}$), Si-II and XI. Experimental uncertainty on lattice parameters is lower than 0.003 Å. Uncertainty on pressure measurement increases from 0.05 GPa at 1 GPa to 2 GPa at 150 GPa.

Above 16 GPa: Si-V, VI, VII and X. From 15.8 GPa, diffraction peaks for the simple hexagonal phase (*sh*; *P6/mmm*, Si-V) were observed in addition to those of the *Imma* phase. The two phases coexist from 15.8 to 16.1 GPa and from 16.3 GPa only the simple hexagonal phase was observed. Figure 5 shows the evolution of Si diffraction patterns at pressure above 16.3 GPa. A two phase Le Bail fit at the transition pressure of the *Imma* and simple hexagonal phases gave lattice parameters $a = 4.748$ Å, $b = 4.479$ Å, $c = 2.551$ Å ($b/a = 0.943$; $c/a = 0.537$) for *Imma*; and $a = 2.563$ Å and $c = 2.381$ Å ($c/a = 0.929$) for simple hexagonal. There was only a small change in volume of ~0.18% between the two phases. The phase transition from *Imma* to simple hexagonal is brought about by a further shift of the Si atoms along the [100] direction to form 6-fold symmetry chains parallel to the *Imma* α-direction/simple hexagonal *c*-direction. In the simple hexagonal structure, there is only one atom per unit cell (Wyckoff position 1a) which has a distorted 8-fold coordination environment (CN = 8; at 16.3 GPa 2×2.386Å, 6×2.553Å).

The simple hexagonal phase (Si-V) has been indexed up to 40.9 GPa. At 42.1 GPa, Si-V is replaced by the coexistence of Si-VI and Si-VII, the first with an orthorhombic (*Cmca*) symmetry and the latter with a hexagonal (*P6$_3$/mmc*) symmetry. This field of coexistence serve as transition to the pure Si-VII stability field that begins at 47.0 GPa (see Table 5). Si-VII is the only phase observed up to a pressure of 90.8 GPa, at which point peaks belonging to the cubic *Fm$\overline{3}$m* make their first appearance together with the hexagonal structure. From 94.0 GPa, only the cubic (Si-X) phase is observed. The resulting compression curves are plotted in Fig. 4 together with previous results. Whereas, the measured lattice parameters and the corresponding pressures are reported in Tables 6 and 7. The obtained stability fields are in agreement with the literature studies[6,10,16]. However, a shift to higher
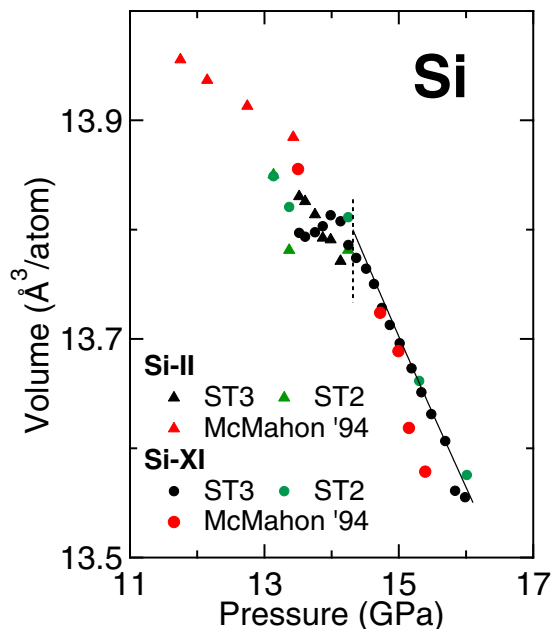
Figure 3. Measured volume of Si-II and Si-XI as a function of pressure (solid black and green marks) compared to previous experimental studies (red solid marks)[6]. The solid line represent a fit of the present experimental data to a Vinet EOS, whereas the dashed line separates the coexistence region from the one phase region.
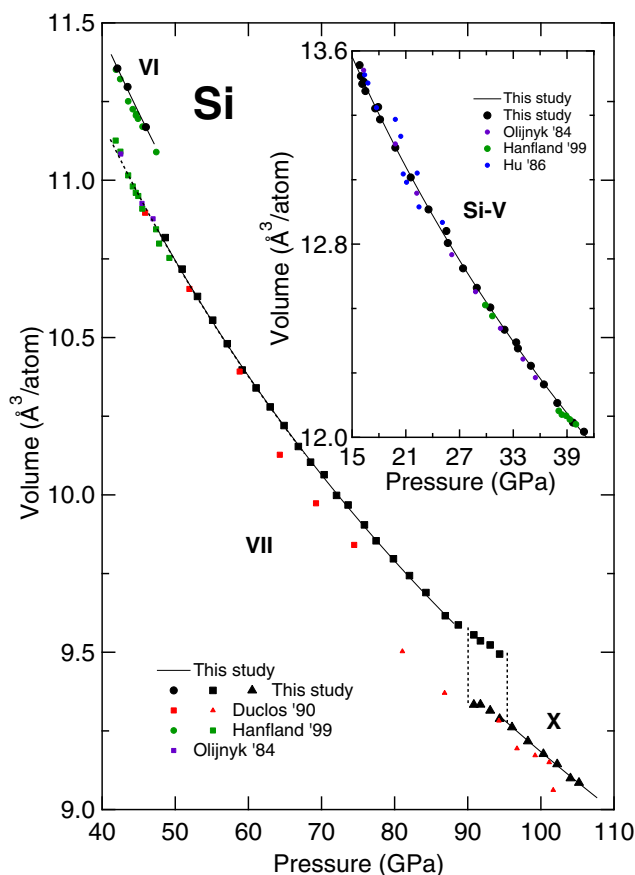
Figure 4. Compression curves of the Si phases observed between 40.0 GPa and 105.2 GPa (inset shows data between 15.0 GPa and 40.0 GPa) and compared to previous studies. Solid black points represent the present experimental data whereas solid black line (with the only exception of the Si-VI) are the corresponding Vinet EOS. The coexistence region between the Si-VI as Si-VII is represented by a dashed line extrapolated from the Si-VII EOS as it was not possible to measure the actual volume of Si-VII having only two peaks. The vertical dashed lines underline the coexistence region between Si-VII and Si-X phases.

P domain	P′ domain	exp. type	PTM	Ref.
Si-V				
15.8–40.9	15.8–40.9	XRD in DAC	He	this
13.2–36.0	13.3–36.9	XRD in DAC	4:1 meth:eth	36
30.0*–40.0	30.6–41.1	XRD in DAC	Ar	16
16.0–34.0**	16.6–37.0	ED-XRD in DAC	4:1 meth:eth	10
15.4–16.2*	15.9–16.8*	XRD in DAC	4:1 meth:eth	6
36.0*–41.0	36.4*-41.7	ED-XRD in DAC	None	17
16.0–33.2		DFT	N/A	19
Si-VI				
42.1–46.0	42.1–46.0	XRD in DAC	He	this
38.0–47.5	39.0–49.0	XRD in DAC	Ar	16
39.0–43.3	39.5–44.0	ED-XRD in DAC	None	17
34.0**	37.0**	ED-XRD in DAC	4:1 meth:eth	10
33.2–40.6		DFT	N/A	19
Si-VII				
42.1–94.4	42.1–94.4	XRD in DAC	He	this
40.0–49.2*	41.1–50.8*	XRD in DAC	Ar	16
36.0–42.0*	36.9–43.2*	XRD in DAC	4:1 meth:eth	36
41.8–79.0	42.4–81.9	ED-XRD in DAC	None	17
40.6–80.0		DFT	N/A	19
Si-X				
90.8–105.2*	90.8–105.2*	XRD in DAC	He	this
79.0–248.0*	81.9–270.0*	ED-XRD in DAC	None	17
80.0–2800.0		DFT	N/A	19

Table 5. Measured pressure domains for phases Si-V, VI, VII and X compared to previous studies. In the table, P refers to the reported pressure domain while P′ is the pressure domain obtained by re-interpreting each reported data using the calibration used in the present study. PTM: Pressure transmitting medium.*: the reported experiment starts or ends at this pressure values. **: Higher pressure are not specified in the reported paper.

transition pressure is observed in the present study (with the only exception of the study of Hanfland et al.[16]). Such a behaviour is attributed to the different hydrostatic condition experienced by the sample in various experiments.

The experimental compression curves for Si-V, Si-VII and Si-X were all fitted with both a Vinet and a BM3 EOS. A fit with the data obtained for the Si-VI phase was not possible as only three data points are available. During the fitting procedure, the V_0 of the high pressure phases have been calculated by extrapolating the data to ambient pressure. The parameters obtained from the fit are reported in Table 8. Concerning the $P6/mmm$ phase, the results obtained from the Vinet and the BM3 fit agrees within the error bars. The observed differences in the absolute values are explained by the trade-off between the bulk modulus and its first derivative in pressure. The lower K_0 in the Vinet is compensated by a higher K_0'. A K_0 smaller than the one of Si-I is consistent with a typical cubic-to-hexagonal structural transition. A similar trend is also obtained for the compression curve of Si-VII, when both equations can be used to describe the experimental data within the error bars. As expected, the fitting parameters for the two hexagonal structures are close to each other with only a minimal reduction of the unit cell volume at higher pressure. In the higher pressure range there is an increment in the bulk modulus value caused by the stabilization of the cubic $Fm\overline{3}m$ phase.

Conclusions

In the present study, the compression curve of Si was investigated from ambient pressure up to 105.2 GPa at ambient temperature using angular dispersive XRD in DAC. The experiment was performed in quasi-hydrostatic conditions using He as pressure transmitting medium. The hydrostaticity of the experiment was qualitatively determined from an analysis of the X-ray diffraction pattern at the highest pressure reached. This showed a maximum deviation from expected lattice parameters, caused by macroscopic stress, of ca. 0.08%, which is within the uncertainty of the experiment. The pressure experienced by the sample was measured via the ruby fluorescence method and from the measured atomic volume of W and Au using the calibration from Dorogokupets et al.[28].

Seven different polymorphs of Si were observed in the investigated pressure range, in agreement with literature data[5–11,16,17,24,25]. The use of He as pressure transmitting medium had not lead to the formation of new Si phases in the investigated pressure range, although a general trend of each phase stability field shifting to higher pressure was observed. In particular, it is important to emphasise the observed behaviour of the well-known Si-I to Si-II phase transition[5–11]. In the present study the Si-II structure was never observed singularly, instead it was found to coexist in the entire pressure domain with the Si-XI phase.
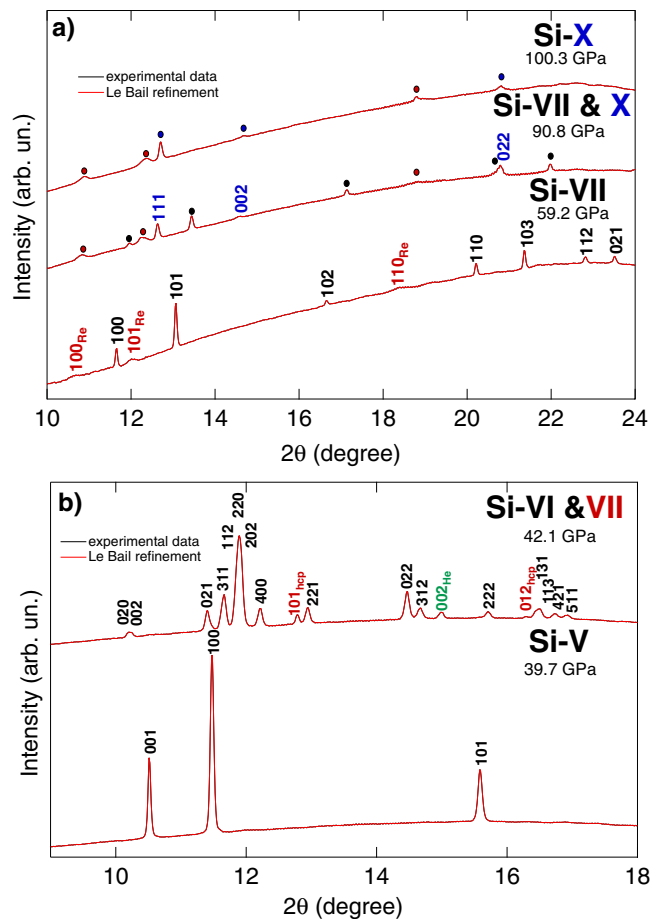
Figure 5. Diffraction patterns of Si collected at (**b**) 39.7 GPa, 42.1 GPa, (**a**) 59.15 GPa, 90.83 GPa and 100.3 GPa. Each pattern has been indexed and the corresponding phase(s) has(have) been specified with different colours. The same colour code is applied to the circle indicating already indexed peaks.

In Fig. 6 the measured compression curve of Si from ambient to 105.2 GPa pressure is reported. The stability fields of the different phases of Si are represented with different colors and filling pattern in the figure. The solid black lines are obtained from the fit of the measured data to Vinet EOS extrapolated down to ambient pressure. The solid line of Si-VII phase starts at 42.1 GPa, even though experimental data for this phase are not reported in the graph. The Vinet EOS curve is extrapolated into the region between 42.1 and 48.6 GPa because in this range Si-VII phase peaks were observed together with the Si-VI phase peaks, indicating their coexistence. However, as the Si-VII phase peaks were not well resolved, it was impossible to include them in a LeBail refinement.

It is interesting to notice how, due to the hydrostatic condition of the actual experiment, four different coexistence regions have been observed in the investigated pressure range. This are: the coexistence between the Si-II and the Si-XI phase in the region between 13.1 GPa and 14.3 GPa; the coexistence between the Si-XI and the Si-V phase between 15.8 GPa and 16.1 GPa; the coexistence between the Si-VI and the Si-VII phase in the region between 42.1 GPa and 46.0 GPa.

The observed coexistence between the Si-VI and the Si-VII phase is in good agreement with the data of Hanfland *et al.*[16] although in their study, they observe a wider stability field for the Si-VI going from a coexistence with the Si-V phase at 38 GPa, to a coexistence with the Si-VII phase starting at 42.5 GPa and ending at above 47.5 GPa when only the Si-VII phase is observed.

The newly observed coexistence between the Si-VII and the Si-X phases in the region between 90.8 GPa and 94.4 GPa was probably not observed by Duclos *et al*. due to the absence of hydrostatic condition during their experiment[17].

Finally, it is important to notice that these coexistence regions do not necessarily describe the thermodinamically stable fields since usually, solid-solid phase transitions (like those observed here) can be strongly affected by kinetic barriers[39]. Therefore, the phase boundaries experimentally determined in the present study might correspond to kinetic phase boundaries[40]. A further characterization of these coexistence region under releasing pressure will provide a better insight on the thermodynamic stability field of these phases.

Run	P_{ruby}[28]	P_{Au}[31]	P_W[28]	a_{Au}	a_W	a_V	c_V	a_{VI}	b_{VI}	c_{VI}	a_{VII}	c_{VII}	a_X
ST1	17.9		17.3		3.112	2.547	2.380						
	25.5		23.3		3.096	2.510	2.357						
	33.3		32.4		3.073	2.476	2.334						
	40.9		39.8		3.056	2.449	2.315						
	43.5		42.5		3.050			7.962	4.774	4.755			
	46.0		45.0		3.045			7.921	4.758	4.742			
	48.6		47.7		3.039						2.451	4.160	
	50.9		50.1		3.034						2.443	4.146	
	53.0		52.3		3.030						2.437	4.135	
	55.1		54.4		3.026						2.431	4.125	
	57.1		56.4		3.022						2.425	4.115	
	59.2		58.6		3.018						2.419	4.105	
	61.1		60.3		3.014						2.415	4.096	
	63.0		62.2		3.011						2.410	4.089	
	64.9		64.3		3.007						2.405	4.081	
	66.8		66.0		3.004						2.400	4.072	
	68.5		67.9		3.000						2.396	4.064	
	70.4		69.9		2.997						2.391	4.064	
	72.1		71.7		2.994						2.388	4.051	
	73.6		73.1		2.991						2.385	4.047	
	75.9		75.2		2.988						2.381	4.036	
	77.5		76.9		2.985						2.376	4.031	
	79.8		79.1		2.981						2.372	4.023	
	82.0		81.2		2.978						2.367	4.015	
	84.3		83.6		2.974						2.363	4.008	
	86.9		86.4		2.969						2.357	3.997	
	88.7		87.8		2.967						2.354	3.994	
	90.8		89.8		2.964						2.352	3.990	3.342
	91.7		90.8		2.962						2.351	3.985	3.342
	93.1		92.1		2.960						2.350	3.981	3.340
	94.4		93.7		2.958						2.349	3.975	3.337
	96.1		95.4		2.955								3.334
	98.2		97.4		2.952								3.328
	100.3		99.3		2.950								3.323
	102.2		101.3		2.947								3.320
	104.0		103.4		2.944								3.314
	105.2		104.2		2.943								3.312
ST3	15.8	15.6		3.978		2.563	2.381						
	16.0	15.7		3.977		2.555	2.387						
	16.1	15.9		3.976		2.554	2.384						
	16.3	16.0		3.974		2.554	2.386						
ST2	16.5	16.8		3.972		2.550	2.385						
	17.6	17.6		3.968		2.545	2.382						
	18.1	18.2		3.965		2.542	2.380						
	19.8	19.8		3.957		2.534	2.375						
	21.6	21.3		3.9500		2.525	2.369						
	23.5	23.4		3.940		2.515	2.362						
	25.7	25.6		3.930		2.505	2.355						
	27.4	27.5		3.923		2.498	2.350						
	28.9	28.8		3.917		2.492	2.346						
	30.4	30.4		3.910		2.486	2.342						
	32.0	32.0		3.904		2.480	2.337						

Table 6. The unit-cell parameters of the high-pressure phases of Si at ambient temperature. All values are obtained using He as pressure transmitting medium. The pressures measured with the ruby fluorescence method and Au and W standards are all reported in GPa. The lattice parameters are reported in Å. Experimental uncertainty on lattice parameters is lower than 0.003 Å. Uncertainty on pressure measurement increases from 0.05 GPa at 1 GPa to 2 GPa at 150 GPa.

Run	P_{ruby}[28]	P_{Au}[31]	P_W[28]	a_{Au}	a_W	a_V	c_V	a_{VI}	b_{VI}	c_{VI}	a_{VII}	c_{VII}	a_X
	33.5	33.4		3.899		2.474	2.333						
	35.0	34.8		3.894		2.469	2.329						
	36.4	36.6		3.887		2.463	2.325						
ST2	37.9	38.0		3.882		2.458	2.321						
	39.7	39.5		3.877		2.452	2.317						
	42.1	42.0		3.868				7.987	4.781	4.758			

Table 7. The unit-cell parameters of the high-pressure phases of Si at ambient temperature. All values are obtained using He as pressure transmitting medium. The pressures measured with the ruby fluorescence method and Au and W standards are all reported in GPa. The lattice parameters are reported in Å. Experimental uncertainty on lattice parameters is lower than 0.003 Å. Uncertainty on pressure measurement increases from 0.05 GPa at 1 GPa to 2 GPa at 150 GPa.

|	This study Vinet	This study BM3
Si-I		
V_0 (Å³/atom)	20.021 (1)	20.011 (1)
K_0 (GPa)	101.5 (3)	101.5 (2)
K_0'	3.43 (5)	3.45 (3)
Si-XI		
V_0 (Å³/atom)	17.04 (6)	17.13 (6)
K_0 (GPa)	45 (7)	42 (6)
K_0'	4 (2)	4 (1)
Si-V		
V_0 (Å³/atom)	15.3 (1)	15.2 (1)
K_0 (GPa)	95 (10)	99 (10)
K_0'	4.6 (5)	5.0 (6)
Si-VII		
V_0 (Å³/atom)	14.3 (1)	14.3 (1)
K_0 (GPa)	96.9 (9)	100.0 (8)
K_0'	4.01 (4)	4.40 (6)
Si-X		
V_0 (Å³/atom)	13.3 (2)	13.3 (2)
K_0 (GPa)	136 (5)	132 (6)
K_0'	4.2 (3)	3.8 (2)

Table 8. EOS parameters of Si-I, Si-V, VII and X as obtained in this experiment from a Vinet and a third-order Birch-Murnaghan (BM3) EOS. The zero pressure volume V_0, bulk modulus K_0, and its pressure derivative K_0' are listed. The EOS formulations are specified.

Methods

The structural evolution of Si from ambient pressure to 105.2 GPa was investigated by synchrotron XRD experiments in DAC at ambient temperature. Four DACs were used during the course of this study, each fitted with a Re gasket. Gaskets were prepared by pre-indenting Re foils (200 μm initial thickness), which were then drilled by spark erosion to form the high-pressure chambers of the cells.

A grain of Si (approx 4 μm each; 99.999% purity, Sigma Aldrich) was loaded into each chamber and a pressure standard was also added a few μm from the Si sample. Ruby spheres were used in all four cells as pressure standards, whilst in three of them an additional W or Au X-ray standard was included since these metals have high X-ray scattering powers and well characterised EOS, attested by the consistency between static, dynamic and ultrasonic measurements[27,41]. Finally the He pressure transmitting medium was loaded into the cell. The experimental conditions adopted in each run are reported in Table 9.

Diffraction data were collected at beamline I15 (Diamond Light Source, Oxon., UK)[42] using a monochromatic X-ray beam ($\lambda = 0.4246$ Å and $\lambda = 0.3099$ Å) and measured using a MAR345 area detector. The detector geometry was calibrated with a La B_6 standard using the powder calibration routines of the DAWN software suite[43]. Measurements were made at three different sample-detector distances (500.39 mm, 424.36 mm and 324.44 mm; determined from DAWN calibration), with the distance selected depending on the angular range necessary to follow changes in the structure under investigation. Masks were applied to the raw diffraction images on a per-image basis before they were azimuthally integrated using the processing tools in the DAWN suite[44]. Diffraction data were analyzed by Le Bail fitting using the routines of the TOPAS software suite[45], literature values for the lattice parameters of each phase were used as a starting point for these refinements.
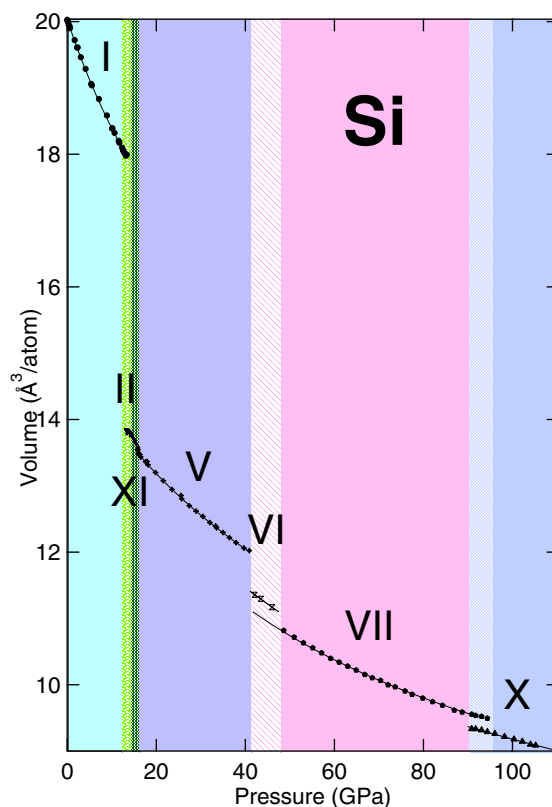
Figure 6. The volume-pressure relation of Si up to 105.2 GPa at room temperature using He as pressure-transmitting medium. Black symbols represents the measured experimental volumes. The continuous black line represent the fit of the experimental data of each phase to a Vinet EOS.

Run	P range	P gauge	culet size	sample size	SDD (mm)	X-rays wavelength (nm)
ST2	0.38–42.1	Ruby, Au	400	3	500.36	0.4246
ST1–2	0.32–13.3	Ruby	150 × 300	3	336.64	0.4246
ST1	0.33–105.2	Ruby, W	150 × 300	4	500.36	0.4246
ST3	2.1–16.3	Ruby, Au	500	3	470.85	0.3099

Table 9. Condition of each experimental run. Sizes are in μ m; pressures are in GPa. All samples were loaded in He pressure transmitting medium. SDD: Sample-to-detector distance.

hkl	d_m(Å)	d_{calc}(Å)	$\frac{d_m - d_{calc}}{d_{calc}}$ %
111	1.91245	1.91243	0.001
002	1.65748	1.65621	0.077
022	1.17065	1.17112	0.040
311	0.99885	0.99873	0.012

Table 10. Measured reflections for Si-X at 105.2 GPa. *hkl* are the Miller indices of the reflection. d_m is the corresponding measured inter-planar distance measured by individual peak fitting. d_{calc} is the inter-planar distance calculated by a fit of the whole diffraction pattern.

During the experiment, pressures inside the high-pressure chambers of the DACs were measured using ruby luminescence and the unit cell volume of either W or Au for runs ST1, ST2 and ST3 and ruby luminescence only for run ST1-2. Calibration data for these three pressure standards were taken from Dorogokupets *et al*.[28]. The entire set of integrated XRD patterns is reported in Figs S1–S3 of the Supplementary Materials.

Hydrostatic conditions. As stated in Takemura and Dewaele[31] and Anzellini *et al*.[29], it is desirable to achieve purely hydrostatic conditions in the sample chamber of a diamond anvil cell, which would be provided by a liquid

pressure transmitting medium. However, even helium becomes solid above about 12 GPa at room temperature and above this pressure, tends to induce non-hydrostatic stress in the sample chamber. Even at lower pressure, the stress can become non-hydrostatic if the sample bridges the anvils due to excessive thinning of the gasket or due to a large initial thickness of the sample. For this reason, interferometry was used to ensure that sample size and indent depth were of the correct relative dimensions to prevent the sample bridging the diamond culets.

A qualitative analysis of the hydrostatic conditions of the sample has been performed by comparing the measured d-spacing of Si at the highest pressure reached (105.2 GPa) to the theoretical (hydrostatic) one calculated using the lattice parameter obtained by a refinement of the entire XRD pattern[26]. Table 10 shows the measured and the calculated d-spacing of Si-X at 105.2 GPa together with their percentage deviation. The deviation of less than 0.08%, is within the experimental error of the present experiment. Such an error was estimated from the deviation between the measured and calculated d-spacing of the LaB_6 standard at ambient pressure. We can thus conclude that the non-hydrostatic stress is below the detection limit of our measurement. This is in agreement with the quantification of the macroscopic non-hydrostatic stress on metals in a helium pressure transmitting medium - i.e. 0.5 GPa at 150 GPa[46].

A similar conclusion is obtained from the analysis of the pressure evolution of the R_1-R_2 splitting and the full width half maximum (FWHM) of R_1 ruby fluorescence peaks (Fig. S6 of the Supplementary Materials (SM)) and the pressure evolution of the FWHM and normalized d-spacing of the W pressure gauge (Fig. S7 of SM), as explained in Takemura[26].

Data availability
All data generated or analysed during this study are included in this published article.

References

1. Poirier, J. *Introduction to the Physics of the Earth's interior* (Cambridge University Press, 1991).
2. Pandolfi, S. *et al.* Nature of hexagonal silicon forming via high-pressure synthesis: nanostructured hexagonal 4h polytype. *Nano Lett.* **18**, 5989 (2018).
3. Alfe, D., Gillan, M. & Price, G. Temperature and composition of the earth's core. *Contemp. Phys.* **48**, 63 (2007).
4. Jamienson, J. Crystal structrure at high pressure of metallic modifications of silicon and germanium. *Science* **139**, 762 (1963).
5. Hu, J., Merkle, L., Menoni, C. & Spain, I. Crystal data for high-pressure phases of silicon. *Phys. Rev. B* **34**, 4679 (1986).
6. McMahon, M., Nelmes, R., Wright, N. & Allan, D. Pressure dependence of the imma phase of silicon. *Phys. Rev. B* **50**, 739 (1994).
7. Piermarini, G. & Block, S. Ultrahigh pressure diamond-anvil cell and several semiconductor phase transition pressures in relation to the fixed point pressure scale. *Rev. Sci. Instrum.* **46**, 973 (1975).
8. Weinstein, B. & Piermarini, G. Raman scattering and phonon dispersion in si and gap at very high pressure. *Phys. Rev. B* **12**, 1172 (1975).
9. Welber, B., Kim, C., Cardona, M. & Rodriguez, S. Dependence of the inderect energy gap of silicon on hydrostatic pressure. *Solid State Commun.* **17**, 1021 (1975).
10. Olijnyk, H., Sikka, S. & Holzapfel, W. Structural phase transitions in si and ge under pressure up to 50 gpa. *Phys. Lett.* **103A**, 137 (1984).
11. Gupta, M. & Ruoff, A. Static compression of silicon in the [100] and [111] directions. *J. Appl. Phys.* **51**, 1072 (1980).
12. Altshuler, L. V. Use of shock waves in high-pressure physics. *Sov. Phys. Usp.* **8**, 52 (1965).
13. Pavloskii, M. Formation of metallic modification of germanium and silicon under shock loading. *Sov. Phys. Solid State* **9**, 2514 (1968).
14. Duval, G. & Graham, R. Phase transitions under shock-wave loading. *Rev. Mod. Phys.* **49**, 523 (1977).
15. McBride, E. *et al.* Phase transition lowering in dynamically compressed silicon. *Nat. Phys.* **15**, 89 (2019).
16. Hanfland, M., Schwarz, U., Syassen, K. & Takemura, K. Crystal structure of the high-pressure phase silicon vi. *Phys. Rev. Lett.* **82**, 1197 (1999).
17. Duclos, S., Vohra, Y. & Ruoff, A. Experimental study of the crystal stability and equation of state of si to 248 gpa. *Phys. Rev. B* **41**, 12021 (1990).
18. Turneaure, S. J., Sharma, S. M. & Gupta, Y. Nanosecond melting and recrystallization in shock-compressed silicon. *Phys. Rev. Lett* **121**, 135701–1 (2018).
19. Paul, R., Hu, S. & Karasiev, V. Anharmonic and anomalous trends in the high-pressure phase diagram of silicon. *Phys. Rev. Le* **122**, 125701 (2019).
20. Zhao, Y., Buehler, F., Sites, J. & Spain, I. New metastable phases of silicon. *Solid State Commun.* **59**, 679 (1986).
21. Crain, J. *et al.* Reversible pressure-induced structural transitions between metastable phases of silicon. *Phys. Rev. B* **50**, 13043 (1994).
22. Wentorf, R. & Kasper, J. Two new forms of silicon. *Science* **139**, 338 (1963).
23. McMahon, M. & Nelmes, R. New high pressure phase of si. *Phys. Rev. B* **47**, 8337 (1993).
24. Senoo, M., Mii, H., Fujishiro, I. & Fujikawa, T. Precise measurements of lattice compression of al, si and al-si alloys by high pressure x-ray diffractometry. *Jpn. J. Appl. Phys.* **15**, 871 (1976).
25. Duclos, S., Vohra, Y. & Ruoff, A. hcp-to-fcc transition in silicon at 78 gpa and studies to 100 gpa. *Phys. Rev. Lett.* **58**, 775 (1987).
26. Takemura, K. Evaluation of the hydrostaticity of helium-pressure medium with powder x-ray diffraction techniques. *J. Appl. Phys.* **89**, 662 (2001).
27. Dewaele, A., Loubeyre, P. & Mezouar, M. Equation of state of six metals above 94 gpa. *Phys. Rev. B* **70**, 094112 (2004).
28. Dorogokupets, P. & Oganov, A. Ruby, metals, and mgo as alternative pressure scales: A semiempirical description of shock-wave, ultrasonic, x-ray, and thermochemical data at high temperature and pressure. *Phys. Rev* **75**, 024115 (2007).
29. Anzellini, S., Dewaele, A., Occelli, F., Loubeyre, P. & Mezouar, M. Equation of state of rhenium and application for ultra high pressure calibration. *J. Appl. Phys.* **115**, 043511 (2014).
30. Katzke, H., Bismayer, U. & Toledano, P. Theory of the high-pressure structural phase transitions in si, ge, sn, and pb. *Phys. Rev.* **73**, 134105, https://doi.org/10.1103/PhysRevB.73.134105 (2006).
31. Takemura, K. & Dewaele, A. Isothermal equation of state for gold with a he-pressure medium. *Phys. Rev. B* **78**, 104119 (2008).
32. Vinet, P., Ferrante, J., Rose, J. & Smith, J. Compressibilty of solids. *J. Geophys. Res.* **92**, 9319 (1987).
33. McSkimin, H. & Andreatch, P. Elastic moduli of silicon vs hydrostatic pressure at 25.0 c and -195.8 c. *J. Appl. Phys.* **35**, 2161 (1964).
34. Hennig, R. *et al.* Phase transformation in si from semiconducting diamond to metallic b-sn phase in qmc and dft under hydrostatic and anisotropic stress. *Phys. Rev. B* **82**, 014101 (2010).
35. Wang, C., Gu, J., Kuang, X. & Xiang, S. Equation of state, nonlinear elastic response, and anharmonic properties of diamond-cubic silicon and germanium: first-principle investigation. *Z. Naturforsch.* **70**((6)a), 403 (2015).
36. Hu, J. & Spain, I. Phase of silicon at high pressure. *Solid State Commun.* **51**, 263 (1984).

37. Takemura, K. & Singh, A. High-pressure equation of state for nb with a helium-pressure medium: Powder x-ray diffraction experiments. *Phys. Rev. B* **73**, 224119 (2006).
38. Yao, Y. & Klug, D. Structural phase transitions in si under hydrostatic and uniaxial compression. *Phys. Rev. B* **85**, 214122 (2012).
39. Errandonea, D. *et al.* Exploring the high-pressure behaviour of the three known polymorphs of bipo4: Discovery of a new polymorph. *J. Appl. Phys.* **117**, 105902 (2015).
40. Bray, A. Theory of phase-ordering kinetics. *Adv. Phys.* **43**, 357–459 (1994).
41. Holzapfel, W. Refinement of the ruby luminescence pressure scale. *J. Appl. Phys.* **93**, 1813 (2003).
42. Anzellini, S. *et al.* Laser-heating system for high-pressure x-ray diffraction at the extreme conditions beamline i15 at diamond light source. *J. Synchrotron Radiat.* **25**, 1 (2018).
43. Basham, M. *et al.* Data analysis workbench (dawn). *J. Synchrotron Rad.* **22**, 853 (2015).
44. Filik, J. *et al.* Calibration and processing of powder-diffraction data in dawn. *preparation* (2017).
45. Coelho, A. Topas and topas-academic: an optimization program integrating computer algebra and crystallographic objects written in c++. *J. Appl. Cryst.* **51**, 210 (2018).
46. Dewaele, A. & Loubeyre, P. Pressurizing conditions in helium-pressure-transmitting medium. *High Press. Res.* **27**, 419 (2007).
47. Dewaele, A., Loubeyre, P., Torrent, M. & Mezouar, M. Compression curves of transition metals in the mbar range: Experiments and projector augmented-wave calculations. *Phys. Rev. B* **78**, 104102 (2008).
48. Mao, H., Xu, J. & Bell, P. Calibration of the ruby pressure gauge to 800 kbar under quasi-hydrostatic conditions. *J. Geophys. Res.* **91**, 4673 (1986).
49. Decremps, F., Belliard, L., Gauthier, M. & Perrin, B. Equation of state, stability, anisotropy and nonlinear elasticity of diamond-cubic (zb) silicon by phonon imaging at high pressure. *Phys. Rev. B* **82**, 104119 (2010).
50. Piermarini, G. P., Block, S., Barnett, J. & Forman, R. Calibration of the pressure dependence of the r1 ruby fluorescence line to 195 kbar. *J. Appl. Phys.* **46**, 2774 (1975).

Acknowledgements

Author contributions

S.A. conceived the experiment(s). S.A., M.T.W., A.K. and D.D. conducted the experiments. S.A., M.T.W., F.M. and H.W. analysed the results. The manuscript is written through the contributions of all authors. All authors have given approval to the final version of the manuscript.

Competing interests

The authors declare no competing interests.

Additional information

Supplementary information is available for this paper at https://doi.org/10.1038/s41598-019-51931-1.

Correspondence and requests for materials should be addressed to S.A.

Reprints and permissions information is available at www.nature.com/reprints.

Publisher's note Springer Nature remains neutral with regard to jurisdictional claims in published maps and institutional affiliations.